Theoretical QTAIM, ELI-D, and hirshfeld surface analysis of the Cu-(H)B interaction in [Cu2(bipy)2B10H10]

ARTICLE *in* THE JOURNAL OF PHYSICAL CHEMISTRY A · NOVEMBER 2013

Impact Factor: 2.69 · DOI: 10.1021/jp405270u · Source: PubMed

6 AUTHORS, INCLUDING:

Varvara V. Avdeeva
Russian Academy of Sciences
50 PUBLICATIONS **161** CITATIONS
SEE PROFILE

Elena Malinina
Russian Academy of Sciences
55 PUBLICATIONS **245** CITATIONS
SEE PROFILE

THE JOURNAL OF PHYSICAL CHEMISTRY A

Article

pubs.acs.org/JPCA

Theoretical QTAIM, ELI-D, and Hirshfeld Surface Analysis of the Cu−(H)B Interaction in $[Cu_2(bipy)_2B_{10}H_{10}]$

Anna V. Vologzhanina,*[†] Alexander A. Korlyukov,[†] Varvara V. Avdeeva,[‡] Irina N. Polyakova,[‡] Elena A. Malinina,[‡] and Nikolai T. Kuznetsov[‡]

[†]A. N. Nesmeyanov Institute of Organoelement Compounds Russian Academi of Sciences (INEOS RAS), Moscow, Russia 119991

[‡]Kurnakov Institute of General and Inorganic Chemistry of the Russian Academy of Sciences, Moscow, Russia 119991

Supporting Information

ABSTRACT: Interaction of $[Cu_2B_{10}H_{10}]$ with 2,2′-bipyridine (*bipy*) afforded a novel binuclear discrete complex of the $[Cu_2(bipy)_2B_{10}H_{10}]$ composition. Two copper(I) atoms coordinate a bridge boron cage through an apical edge and a triangular BBB face situated at its opposite apical vertices to form four 3c2e (CuHB) and one 2c2e Cu−B bonds. The charge density model was obtained by density functional theory calculations of isolated molecule and crystal. The resultant densities were analyzed using the quantum theory of atoms in molecules (QTAIM) and electron localizability indicator (ELI-D). The geometry and the topological parameters of copper(I) coordination environment were found to be sensitive to crystal-field effect. An annulus of flat electron density $\rho(r)$ and small $\nabla^2\rho(r)$ is formed at dianion faces. As a result, some of the expected B−B, Cu−B, or Cu−H bond critical points are absent. The topological instability in the region of multicentered bonds is observed. The Cu−B bonding was found to be presumably electrostatic in nature, which could be the reason of topological isomerism for copper(I) decaborates. The results show that an unambiguous real-space criterion for multicentered bonding between transition metals and polyhedral boron anions is not yet given. The molecular graph for this class of compounds does not provide a definitive picture of the chemical boding and can be complemented with other descriptors, such as virial graphs and the ELI-D distribution.

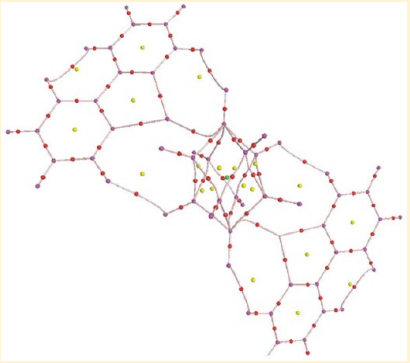

1. INTRODUCTION

Polyhedral boron dianions $B_nH_n^{2-}$ (n = 10, 12) act with metal ions as polydentate ligands and soft reducing agents.[1] Boron atoms of *closo*-decaborate and *closo*-dodecaborate form convex polyhedra through the BBB deltahedral faces. Properties of the dianions are governed by the multicentered electron-deficient bonding in the boron cage. The presence of 3c2e bonds results in high delocalization of electrons over the BBB surfaces.[2−9] The tendency of boron atoms to form multicentered bonds is also observed for complex compounds containing polyhedral boron anions. To date, the structures of about 50 complexes containing polyhedral boron dianions have been published. Investigation of the complexes between a transition metal and a boron claster anion[10−12] revealed that metal bonding to a cage vertex in the $B_nH_n^{2-}$ (n = 6, 10, 12) cluster can be accomplished in three ways. The most widespread is a 3c2e MHB bonding with ∠MHB $\delta \sim 90°$, a 3c2e bonding through bridging hydrogen (M−H(B), ∠MHB ∼ 120°), and a 2c2e M−B bond without participation of the terminal H atom (∠MHB ∼ 60°) also occur. On the example of lead(II) compounds, it was stated that a change in the type of bonding is accompanied by changes in the FTIR spectra.[12] The number of multicentered bonds and their lengths depend on the nature of a polyhedral anion, the nature and the charge of a metal ion, and coordination mode of the dianion.[13]

Coordination chemistry of polyborate-containing complexes attracts much interest due to their ability to form numerous position isomers.[14] First of all, a cation can coordinate a cage through a vertex, an edge or a face. Second, a polyhedral boron anion can realize different coordination modes to form a bridge between two metal atoms. At last, in contrast with $B_6H_6^{2-}$ and $B_{12}H_{12}^{2-}$ anions, apical and equatorial vertics of decahydro-*closo*-decaborate ($B_{10}H_{10}^{2-}$) are not equivalent. Mono- and diprotonated boranes ($B_6H_7^-$, $B_{10}H_{11}^-$, and $B_{10}H_{12}$) can be regarded to some extent as analogues of coordination isomers. X-ray investigations[7] and theoretical calculations[15] of $B_6H_7^-$ species proved that the additional proton H* is situated above a BBB face. Disposition of the H* above a triangular face in the region of an apical boron atom in the $B_{10}H_{11}^-$ anion was also proved theoretically[16] and experimentally.[17] Mebel at al. demonstrated that a barrier for hydrogen migration around the apical region in the $B_{10}H_{11}^-$ is just 2 kcal/mol.[16] Recently Kochnev et al. calculated $B_{10}H_{12}$ species.[18] The five most stable isomers correspond to disposition of two additional H* protons in the region of apical B1 and B10 atoms. The exact disposition includes a face−face, face−edge and edge−edge

Received: May 28, 2013
Revised: November 4, 2013
Published: November 7, 2013

   dx.doi.org/10.1021/jp405270u | *J. Phys. Chem. A* 2013, 117, 13138−13150

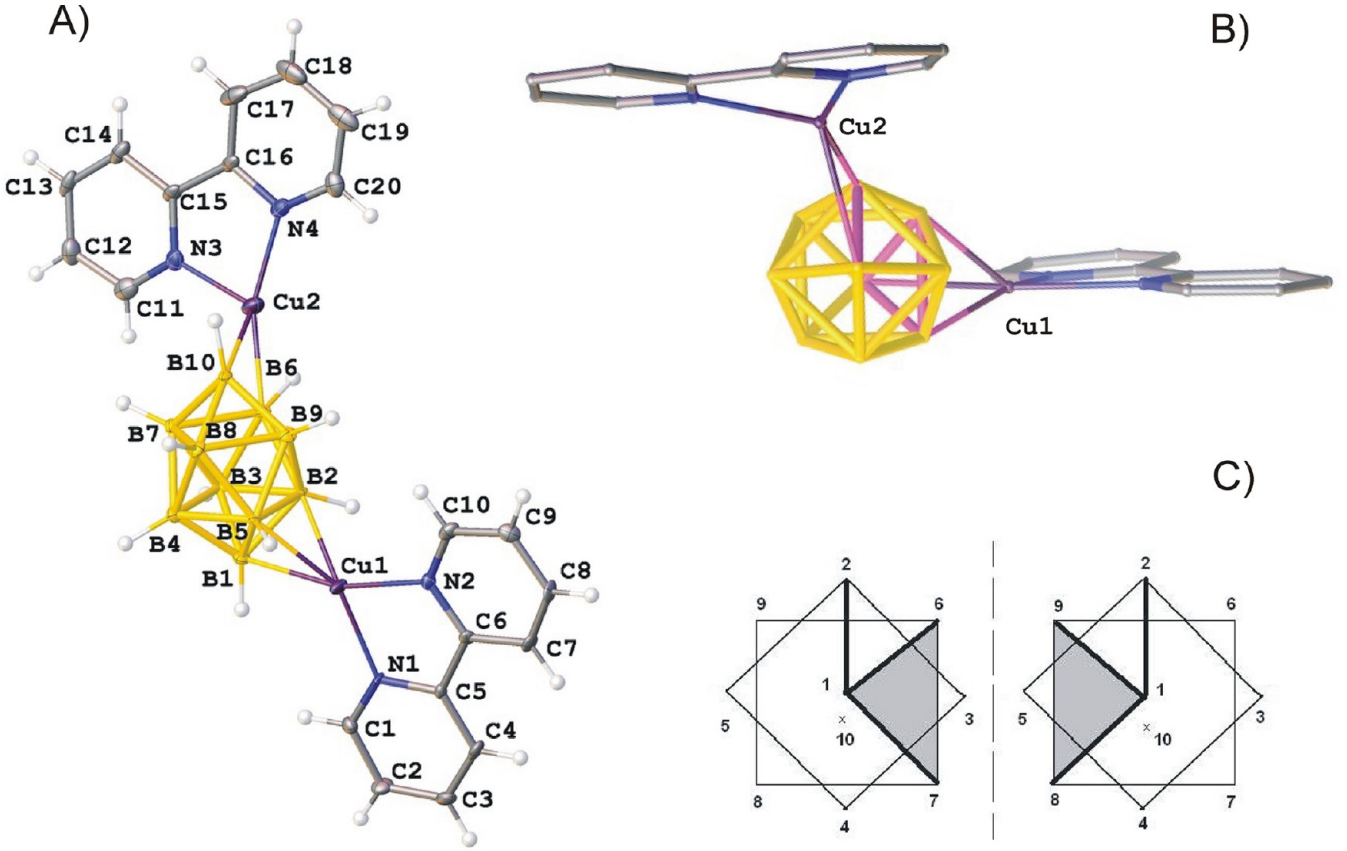

Figure 1. General view of **1**, represented in thermal ellipsoids (depicted at 50% probability level (A)), molecular view along B1···B10 axis (H atoms are not depicted, the B−B edge and face involved in Cu···borate bonding are highlighted with magenta (B)) and schematic representation of its 1−2, 6−7−10 and 1−2, 8−9−10 enanthiomeric forms (C).

coordination. The difference between the full energies of these five isomers does not exceed 4 kcal/mol.

The family of copper(I) decahydro-*closo*-decaborates clearly demonstrates above-mentioned isomerism. The majority of compounds realize (CuBH) coordination, for example, a family of chain borates with the $\{Cat[CuB_{10}H_{10}]\}_n$ composition (Cat = K^+, Cs^+, $R_{4-n}NH_n^+$ (n = 0, 1, 2; R = Me, Et, Pr, n-Bu), Ph_4P^+, Ph_4As^+, $(C_{11}H_9)Ph_3P^+$ ($C_{11}H_9$ = $NaphCH_2^-$ = α-methyl-naphthyl-),[11,19] while the Cu−H(B) bonds were found at $[(Cu^{II}_4 bipy_4(OH)_4(B_{10}H_{10})_2(DMSO)_2$[20] and $\{[(Cu^{II}_4 bipy_4(OH)_4][Cu^{I}_2(B_{10}H_{10})_3]\}\cdot 4CH_3CN$.[21] Isomerism in the case of the bridge cage is represented by coordination modes through (i) the apical and equatorial edges (1−2,3−7 isomer for $Cs[CuB_{10}H_{10}]$[10] and the 1−2,5−8 isomer for $(C_2H_5)_3NH[CuB_{10}H_{10}]$),[11] (ii) two apical edges (1−2,6(9)-10 at $[Cu_2(Ph_3P)_4B_{10}H_{10}]$,[22,23] 1−2,7(8)−10 coordination at $(CH_3)_2NH_2[CuB_{10}H_{10}]$[10] or $[Cu_2(9Nphen)_4B_{10}H_{10}]$[24] and 1−2,1−4 for another isomer of $[Cu_2(9Nphen)_4B_{10}H_{10}]$),[24] or (iii) equatorial vertices at $Ph_4P[Cu(B_{10}H_{10})]$.[25] Schematic numeration of boron atoms in the cage is given in Figure 1B, and principles of notation of coordination mode for boron claster anions are given by Drozdova, et al.[14] The copper compounds that exhibit face coordination of the cage have not been obtained up to date, the edge-coordination of the decaborane cage by means of two (CuBH) bonds dominates over the rest coordination modes. Thus, predominance of edge-coordination raises the question about its reason. In this view, the nature of the Cu−B bonding at copper(I) decaborates becomes of particular interest.

The QTAIM[26] is a powerful tool to investigate the chemical bonding between atoms on the basis of the topological properties of the electron density distribution function (ρ(r)) and the associated Laplacian ($\nabla^2\rho(r)$). The electron localization function (ELF)[27] and the electron localizability indicator (ELI-D)[28] can also be used for investigation of multicenterd bonds to distinguish bonded electrons, core electrons and lone electron pairs.

Up to date the QTAIM study has been carried out of some polyhedral boranes,[3−7,9,29−32] and complexes containing M-(η^5-C_2B_3) bonding: $[NMe4][3,3'\text{-}Co(1,2\text{-}C_2B_9H_{11})_2]$,[33] $[3\text{-}(\eta^5\text{-}C_5Me_5)\text{-}1,2\text{-}(PhCH_2)_2\text{-}closo\text{-}3,1,2\text{-}RhC_2B_9H_9]$ and $[3\text{-}\{(1-3\text{-}\eta^3)\text{-}C_8H_{13}\}\text{-}1,2\text{-}(4'\text{-}MeC_6H_4)_2\text{-}pseudocloso\text{-}3,1,2\text{-}RhC_2B_9H_9]$.[34] A number of DFT calculations were published for comparative analysis of stable isomers for compounds containing M-B bonding, for example, $[1,1,1\text{-}(PMe_3)_2H\text{-}IrB_8H_7\text{-}8\text{-}Cl]$,[35] $Cp^*_2Ru_2(B_8H_{14})$,[36] isomers of 4-(η-$C_{10}H_8$)-**4**,1,*n*-*closo*-$MC_2B_{10}H_{12}$ (n = 6, 8, 10, 12; M = Ru,[37] Fe[38]), $[(H)_2Cl(PMe_3)_2M(\sigma\text{-H-BR})]$ (M = Fe, Ru, Os; R = OMe, NMe_2, Ph).[39] Regions of high value of ELF have the form of the dual polyhedron of the boron cage.[40,41] Besides, the QTAIM and ELI-D were applied to investigate bonding in isolated boron clasters,[42] and crystalline MB_6 (M = Na, K, Rb, Ca, Sr, Ba, Sc, Y, La)[43] and $(NH_4)_2(B_6H_6)$.[44] To the best of our knowledge neither the QTAIM, nor ELI-D investigation of complexes containing d-elements and *closo*-decaborate dianion as well as description of crystal packing effect for these compounds has not been carried out before.

dx.doi.org/10.1021/jp405270u | J. Phys. Chem. A 2013, 117, 13138−13150

Herein we present the synthesis, the structure, and theoretical charge density study of a novel molecular compound of a $[Cu_2(bipy)_2B_{10}H_{10}]$ composition (**1**). The compound was found to be the first representative of copper(I) decaborates with the mixed edge-face coordination of the bridge dianion; thus, peculiarities of Cu−B bonding for this compound became of particular interest. Weak reflection ability of the compound did not allow obtaining experimental $\rho(r)$ using multipole refinement. The $\rho(r)$ function in the crystal (*cry*) of **1** was obtained by means of plane-wave DFT (PW-DFT) calculations and compared with that for the isolated molecule (*gas*).

2. EXPERIMENTAL SECTION

Tris(ethyl)amine, 1,2′-bipiridinium, and solvents were obtained commercially (Aldrich). Solvents were distillated before synthetic procedures. $(Et_3NH)_2[B_{10}H_{10}]$ was obtained by a known procedure[45] from decaborane-14 through a 1,6-*bis*(*tris*(ethyl)amin)decaborane. Copper(I)-decahydro-*closo*-decaborate $[Cu_2B_{10}H_{10}]$ was obtained by interaction of $(Et_3NH)_2B_{10}H_{10}$ and $CuSO_4$ as described in ref 19.

The IR spectra of the solid sample (NaCl tablets) in the range 600−4000 cm^{-1} were recorded with a FT-IR InfraLum FT-02 (Lumex) spectrophotometer. Analytical data (C, H, N content) of dried compounds were obtained with a Carlo Erba model EA1108 microanalyzer. Boron content was determined with a Perkin-Elmer Model 2100 atomic absorption spectrophotometer with electro-thermal atomizer HGA-700.[46]

Preparation of $[Cu_2bipy_2B_{10}H_{10}]$ (1). Complex $[Cu_2B_{10}H_{10}]$ (0.01 mol) was dissolved in acetonitrile (10 mL) and a solution of 2,2′-bipyridyl (0.02 mol) in acetonitrile (10 mL) was added to the reaction mixture. The dark-red coloration of the mixture immediately appeared and red crystalline precipitate formed. The solid residue was filtered off and dried on air. Yield: 85%. Anal. Calc. for $C_{20}H_{26}B_{10}Cu_2N_4$ (%): Cu, 22.53; C, 43.19; H, 4.78; N, 10.09; B, 19.41. Found (%): Cu, 22.79; C, 43.08; H, 4.70; N, 10.05; B, 19.39. IR (NaCl) ν/cm^{-1}: 2486 ν(BH); 2066 $\nu(BH)_{MHB}$; 1005 δ(BBH); 1605−700 ν(*bipy*).

Crystallographic Measurements. The red colored needle shaped crystal of the complex $[Cu_2bipy_2B_{10}H_{10}]$ was obtained from the reaction mixture. The crystal system of $C_{20}H_{26}B_{10}Cu_2N_4$ (M = 557.63) is monoclinic; at 100.0(2) K: a = 15.5479(11) Å, b = 10.6631(8) Å, c = 14.8450(11) Å, β = 101.674(1)°, V = 2410.2(3) Å^3, space group *Cc*, Z = 4, D_{calc} = 1.537 g cm^{-3}, μ = 1.78 mm^{-1}. The intensities of 15168 reflections were measured with a Bruker Apex 2 CCD using graphite monochromated Mo−Kα radiation (λ = 0.71073 Å, 2θ < 52°). 4683 independent reflections ($R(int)$ = 0.027) were used for the solution and the refinement. The structure was solved by direct methods and optimized by full-matrix least-squares refinement against F^2. Non-hydrogen atoms were found on difference Fourier maps and refined with anisotropic displacement parameters. The positions of hydrogen atoms were calculated and included in the refinement in isotropic approximation with the $U_{iso}(H) = 1.2U_{eq}(X_i)$, where $U_{eq}(X)$ are equivalent thermal parameters of the parent atoms. Positions of H(B) atoms situated near copper atoms (H2, H5, H6 and H10) were refined with B−H distances fixed at 1.12 Å, the rest hydrogen atoms were refined by the riding model (using HFIX 153 instruction). The final convergence factors for **1** were $R_1(F)$ = 0.051 for 3932 reflections with $I > 2\sigma(I)$, wR_2 = 0.113, and GOF = 0.99 for all the independent reflections. All calculations were performed using the SHELXTL PLUS 5 program package.[47]

There is a high residual electron density of 4.0 e Å^{-3} at 2.0 Å near B10 atom (and 2.2 Å from B8), probably, due to the presence of twinned component. Unfortunately, it was impossible to find a single crystal of better quality or to separate components of a twinned crystal and to refine the structure using HKLF/BASF instructions. Attempts to separate two components with PART instructions and refine site occupancy lead to unstable refinement.

CCDC 940613 contains the supplementary crystallographic data for this paper. These data can be obtained free of charge via http://www.ccdc.cam.ac.uk/conts/retrieving.html or from the Cambridge Crystallographic Data Centre, 12 Union Road, Cambridge CB2 1EZ, UK; fax: (+44) 1233 336 033; or e-mail deposit@ccdc.cam.ac.uk.

Quantum-Chemical Calculations. The quantum chemical calculations of the crystalline state of **1** were carried out using the Vienna Ab-initio Simulation Package (VASP) 4.6.28 code.[48−50] Conjugated gradient technique was used for optimizations of the atomic positions (started from experimental data) and minimization of total energy. Projected augmented wave (PAW) method was applied to account for core electrons while valence electrons were approximated by plane-wave (PW) expansion with 545 eV cutoffs. Exchange and correlation terms of total energy were described in terms of density functional theory (DFT). PBE exchange-correlation functional was used for this purpose.[51] At a final step of our calculations atomic displacements converged were better than 0.01 eV·Å^{-1}, as well as energy variations were less than 10^{-3} eV. In order to carry out the topological analysis of electron density distribution function in terms of AIM theory the dense (360 × 240 × 336 points) FFT (fast Fourier transformation) grid was used. The latter was obtained by separate single point calculation of optimized geometry with small core PAWs for each atom type. The topological analysis of electron density distribution function was carried out using the AIM program − part of the ABINIT software package.[52]

Quantum chemical calculations of isolated molecules were carried out using Gaussian 03 program suite.[53] All atoms were treated using PBE0/6-311G(d,p) functional and basis set combination. The topological analysis was performed by means of the AIMALL program package.[54]

Calculation and analysis of ELI-D function was carried out using the DGRID 4.6 program,[55] and the ELI-D basins and isosurfaces were visualized using the ParaView program.[56]

3. RESULTS AND DISCUSSION

3.1. Structural Description of $[Cu_2bipy_2B_{10}H_{10}]$ (1). The structure and composition of complex **1** were obtained with X-ray investigation. A molecular view of the compound is given in Figure 1. Each Cu(I) atom coordinates a *bipy* molecule and a $B_{10}H_{10}^{2-}$ dianion. Both *bipy* molecules act as bidentate-chelate ligands. The dianion is coordinated by copper(I) atoms through its apical edge and opposite apical polyhedron face (coordination of a boron claster anions by a copper atom through a face has not been observed before). In accordance with notation suggested by Drozdova, et al.,[23] the dianion realizes (1−2, 6−7−10) coordination mode (Figure 1B, numeration of boron atoms in the asymmetric unit does not coincide with this schematic labeling). Taking into account the presence of glide plains, the crystal structure of **1** also contains the (1−2, 8−9−10)-coordinated enanthiomer. Selected bond

Table 1. Selected Distances in the Structure of $[Cu_2bipy_2B_{10}H_{10}]$ (Å)[a]

bond	*exp*	*cry*	*gas*	bond	*exp*	*cry*	*gas*
Cu1−N1	2.026 (5)	2.023	2.055	Cu1−H1	2.45	2.46	2.41
Cu1−N2	2.075 (5)	2.051	2.077	Cu1−H2	2.19	2.27	2.17
Cu2−N3	2.064 (5)	2.064	2.074	Cu1−H5	2.15	2.08	2.18
Cu2−N4	2.019 (5)	2.006	2.051	Cu2−H6	1.63	1.71	2.10
Cu1−B1	2.247 (7)	2.186	2.146	Cu2−H7	3.21	3.28	2.24
Cu1−B2	2.256 (7)	2.225	2.146	Cu2−H10	2.19	2.27	2.41
Cu1−B5	2.156 (7)	2.138	2.156	*av.* N−C	1.334	1.350	1.337
Cu2−B6	2.119 (7)	2.091	2.126	*av.* C−C	1.383	1.394	1.389
Cu2−B7	2.980 (7)	2.976	2.184	*av.* B_a−B_e	1.725	1.733	1.718
Cu2−B10	2.349 (7)	2.277	2.151	*av.* B_{e1}−B_{e1}	1.843	1.838	1.838
B3−H3, B4−H4, B8−H8, B9−H9	1.12	1.20	1.19−1.20	*av.* B_{e1}−B_{e2}	1.807	1.800	1.803
B1−H1, B2−H2, B5−H5, B6−H6, B7−H7, B10−H10	1.12	1.20−1.26	1.20−1.21				

[a]The N−C, C−C, B_a−B_e, B_{e1}−B_{e1}, and B_{e1}−B_{e2} distances were averaged. B_{e1}−B_{e1} and B_{e1}−Be2 are the distances between boron atoms within a square antiprism base and those connecting the bases, respectively.

lengths (d) are listed in Table 1. The Cu2−B10 bond length is elongated to 2.349(7) Å, *d*(Cu2−H6) = 2.66 Å, and the angle Cu2−H10−B10 is 62°, the latter value is characteristic for 2c2e Cu−B bonding. The rest Cu−B and Cu−H distances vary from 2.119(7) to 2.256(7) and from 1.64 to 2.45 Å. Taking into account Cu−H−B angles of ∼90°, the Cu2−B6, Cu1−B1, Cu1−B2, and Cu1−B5 bonds are of 3c2e (CuHB) type.

3.2. DFT Calculations. *3.2.1. Geometry.* The main intramolecular distances of the complex in the gas phase (*gas*) and the crystal (either experimental (*exp*) and PW-DFT calculated (*cry*)) are listed in Table 1. Let us denote the capping B atoms as B_a, whereas the B atoms within the square antiprisms are labeled as B_e. All N−C, C−C, B_a−B_e, and B_e−B_e distances were averaged. The distances of these covalent bonds remain almost constant for *exp*, *cry*, and *gas* models. At the same time, the lengths of coordination bonds for both copper(I) atoms (Table 1) in the isolated molecule significantly vary from that in the crystalline state. In *gas*, all six Cu−B bonds and four Cu−N bonds are close to each other (2.126−2.184 and 2.051−2.077 Å); the boron claster dianion is coordinated through two faces (Figure 2, Table 1). In the crystalline state (*exp* and *cry* models) the reorganization of Cu−B distances is unambiguously observed, in particular the increase in the Cu2−B7 distance from 2.13 to 2.98 Å is corresponded by the change in coordination mode of the dianion (from face−face to edge-face). Besides, the Cu−N bonds become alternated (2.006−2.026 and 2.051−2.075 Å) so that elongation (weakening) of a Cu−B bond length is corresponded by shortening (strengthening) of the trans-situated Cu−N bond. Thus, in contrast with *bipy* and $B_{10}H_{10}^{2-}$ species, the geometry of coordination node in **1** was found to be highly sensitive to the effects of crystal packing.

All covalent bonds calculated by PW-DFT are longer, and calculated coordination bonds are shorter in comparison with those experimentally observed (Table 1). Nevertheless, the difference between them does not exceed 0.01 Å. Hence, PW-DFT calculation is a reliable approximation of experimental electron density.

3.2.2. Bonding Interactions in ***1****.* In Figure 2 we represent theoretical graphs of isolated molecule in the scalar field of the electron density $\rho(r)$ (molecular graph) and the potential energy density $V(r)$ (virial graph). The molecular and virial graphs of a molecule were found to be homeomorphic in general with an exception of systems close to catastrophe points.[57] As it can be seen, all expected B−H, C−H, C−C, N−

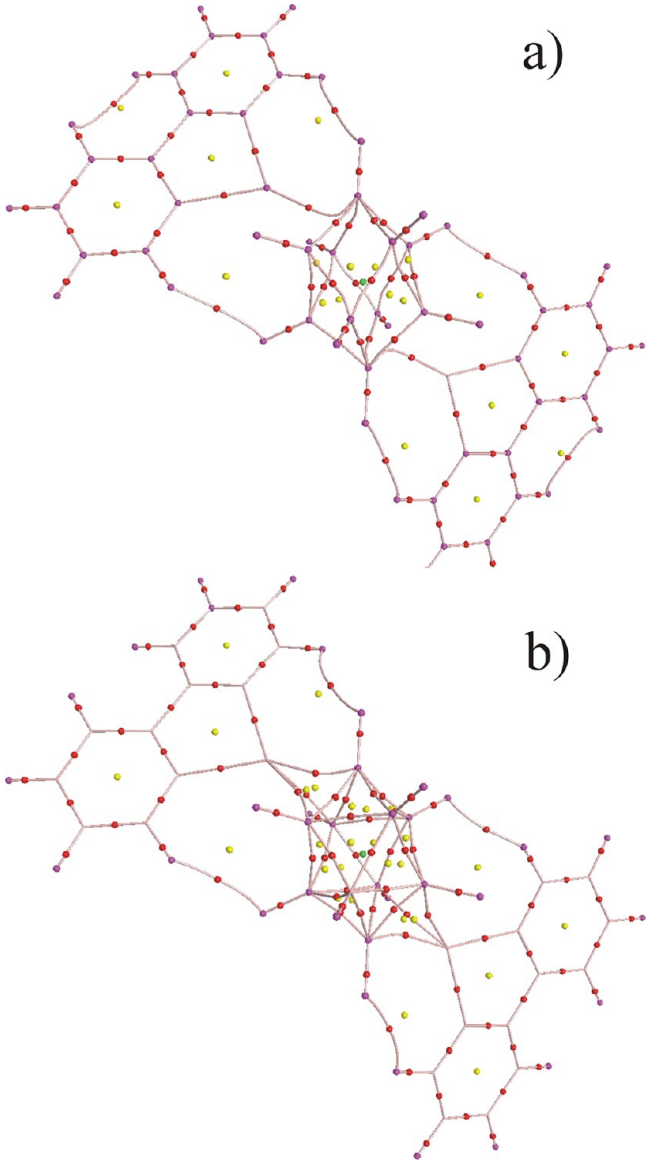

Figure 2. Theoretical graphs of the isolated **1** in the scalar fields of (a) the electron density $\rho(r)$ (molecular graph) and (b) the potential energy density $V(r)$ (virial graph), obtained using AIM2000.[63] The critical points are color-coded: (3; +3) cp's in green, rcp's in yellow, and bcp's in red.

dx.doi.org/10.1021/jp405270u | J. Phys. Chem. A 2013, 117, 13138−13150

Table 2. Selected Topological Parameters of $\rho(r)$ Function for Intramolecular Bonds in 1[a]

bond	d_1, Å	d_2, Å	$\rho(r)$, e Å^{-3}	$\nabla^2\rho(r)$, e Å^{-5}	$V_e(r)$, a.u.	$H^e(r)$, a.u.	ε_{bcp}
Cu1−N1	0.994	1.029	0.61	8.45	−0.13	−0.02	0.09
	0.989	1.062	0.52	8.38	−0.12	−0.01	0.05
Cu1−N2	1.006	1.044	0.57	7.89	−0.12	−0.02	0.12
	1.001	1.076	0.52	8.32	−0.12	−0.01	0.05
Cu1−B1	1.199	1.130	0.47	3.16	−0.08	−0.02	8.12
	1.087	1.300	0.48	3.33	−0.08	−0.02	0.72
Cu2−N3	1.015	1.048	0.56	7.82	−0.12	−0.02	0.04
	1.000	1.074	0.49	7.75	−0.11	−0.01	0.05
Cu2−N4	0.986	1.018	0.63	9.02	−0.14	−0.02	0.19
	0.990	1.062	0.49	7.80	−0.11	−0.01	0.05
Cu2−H6 (*cry*)[b]	0.716	1.038	0.59	5.13	−0.12	−0.03	1.71
Cu2−B10 (*gas*)	1.087	1.339	0.48	3.36	−0.08	−0.02	1.24
av. B_a−B_e	0.864	0.861	0.86	−3.46	−0.17	−0.10	1.69
	0.862	0.875	0.86	−3.43	−0.12	−0.09	2.01
av. B_{e1}−B_{e2}	0.905	0.899	0.77	−2.65	−0.14	−0.09	2.09
	0.917	0.907	0.76	−2.61	−0.10	−0.06	2.28
av. B−H···H−C	1.226	1.116	0.05	0.48	−0.003	0.001	0.26
	1.253	1.107	0.05	0.46	−0.003	0.001	0.22
av. C−H···H−C	1.090	1.090	0.08	1.05	−0.01	0.002	2.02
	1.208	1.209	0.07	0.94	−0.01	0.001	0.93

[a]For all bonds d_1 and d_2 are the distances from atoms x and y to the bcp; $\rho(r_{bcp})$ is the ED at the bcp; $\nabla^2\rho(r_{bcp})$ is the corresponding Laplacian; $V_e(r)$ is potential energy density; ε_{bcp} is bond ellipticity [$\varepsilon_{rcp} = \lambda_1/\lambda_2 - 1$; $\lambda_1 > \lambda_2$]; $H^e(r)$ is local energy density. The first and the second lines give values for PW-DFT (*cry* model) and PBE0/6-311G(d,p) (*gas* model) data, respectively. [b]The Cu2···anion interaction is represented as Cu2−H6 and Cu2−B10 bonds for the *cry* and *gas* models.

Table 3. Averaged Topological Descriptors of rcp's[a]

type[b]	$\rho(r_{rcp})$, e Å^{-3}	$\nabla^2\rho(r_{rcp})$, e Å^{-5}	λ_1, e Å^{-5}	ε_{rcp}[c]	*av.*[c]
Cu-*bipy*	0.18	3.26	−0.50	1.86	4
B_a−B_e−B_e−B_e	0.70	−0.95	−2.91	0.72 + 4.50 + 2.13	6 + 1 + 1
				0.39 + 2.71	6 + 2
py	0.17	4.12	−0.50	0.04	8

[a]For all cases $\rho(r_{rcp})$ is the ED at the rcp; $\nabla^2\rho(r_{rcp})$ is the corresponding Laplacian; λ_1 is the curvature of the ED perpendicular to the ring plane; ε_{rcp} is the ring plane ellipticity [$\varepsilon_{rcp} = \lambda_2/\lambda_3 - 1$; $\lambda_2 > \lambda_3$]; *av.* is the number of averaged rings. [b]The five-membered chelate Cu−N−C−C−N and six-membered NC_5 rings of bipy molecules are labeled as Cu-*bipy* and *py*. [c]ε_{rcp} and corresponding *av.* values are divided with plus sign provided that ε_{rcp} values significantly vary from each other. The first and the second lines give values for PW-DFT (*cry* model) and PBE0/6-311G(d,p) (*gas* model) data.

C, and Cu−N bonds are observed for both graphs. Additionally, four and three intramolecular C−H···H−B contacts as well as two C−H···H−C interactions are present on *gas* and *cry* molecular graphs (Table S1, Supporting Information). In the case of the *gas* molecular graph, the number of observed multicentered bonds (both for copper and boron atoms) is significantly less than expected. Each copper atom forms only one bond path with the dianion. The Cu−B bond paths are very curved, so their lengths are 0.14−0.28 Å longer then corresponding interatomic distances. Additionally, no bond paths were found between the B_e atoms within the same square plane of the antiprism; a folded four-membered ring (B_{e1}−B_a−B_{e1}−B_{e2}) is formed instead. The same trends are observed in the *cry*, although Cu2 is connected with H6 atom. Previously the absence of some of expected bond paths was demonstrated for both the boron claster anions,[4,7,8,30] and a number of transition metal complexes with carbocyclic rings,[58−60] norbornadene[61] or 1-ethynyl-cyclohexan-1-ol.[62] On the virial graph of *gas*, a number of "missing" Cu−B and B−B bond paths are present, but both C−H···H−C contacts are absent. The Cu−B bond critical points (bcp's) on the virial graph are close to CuBB ring critical points (rcp's). It is worth mentioning that Cu−B bond paths are less curved than on the molecular graph. The absence of homeomorphism between molecular and virial graphs as well as the character of Cu−B bond paths indicate that the atomic system is close to catastrophe point.[57]

For both molecular and virial graphs, bcp's corresponding to coordination Cu−N and Cu−B interactions were found approximately in the middles of corresponding bond paths (Figure 2, Table 2). The same is true for C···C and C−H···H−C intermolecular contacts (Table S1, Supporting Information). In the case of B−H, C−H, B···H, and C···H interactions, the bcp's calculated from $\rho(r)$ are shifted toward the positively charged atom. The bcp's corresponding to both inter- and intramolecular B−H·H−C contacts are slightly shifted to *bipy* molecules (Tables 2 and S1, Supporting Information). It could also be expected taking the charges of hydrogen atoms into account. The H(C) atoms are slightly positive, while the H(B) atoms are negatively charged (Table 5, section 3.2.6).

3.2.3. Bond Topology and Electron Distribution in the B−B−B and Cu−H−B Ring Planes. Table 2 displays the bond topological parameters for the main bcp's found in **1**. Values for eight B_a−B_e, eight B_e−B_e bcp's, and intramolecular B−H···H−C interactions are averaged because they showed no significant differences. The agreement between above-mentioned averaged values for the *cry* and *gas* models is good, which points toward

dx.doi.org/10.1021/jp405270u | J. Phys. Chem. A 2013, 117, 13138−13150

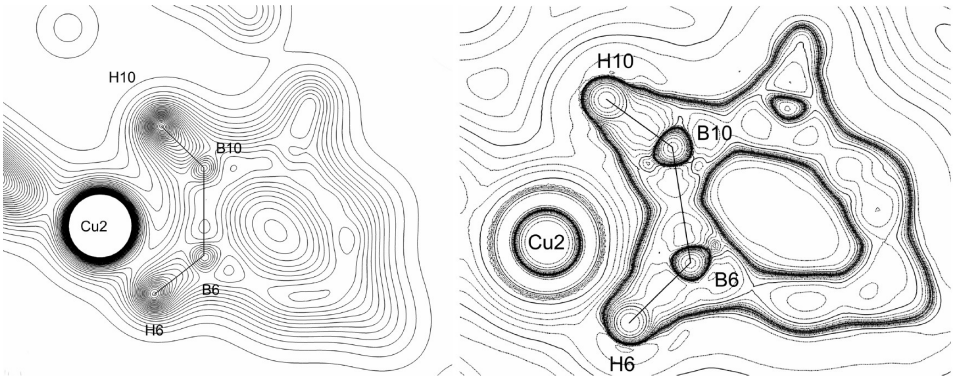

Figure 3. $\rho(r)$ (left) and Laplacian (right) maps of the Cu2−B6−B10 triangle of the *cry* model. Contours of the electron density are depicted at the 0.1 e Å^{-3} level. Positive contours of $\nabla^2\rho(r)$ are given in logarithm scale as solid lines, and negative contours are dashed lines.

Table 4. ELI-D Bond Descriptors of Copper and Borane Bonds

basin	contributed atoms	contribution, %	vol, Å	ELI_{pop}, e	E_{max}, γ	ΔELI, Å
B8−B10	B8, B10	45.3, 54.7	1.34	0.66	1.53	0.50
B1−B4	B1, B4	54.8, 45.2	1.49	0.72	1.53	0.44
B2−B6	B2, B6	48.5, 51.5	1.98	0.86	1.49	0.12
B4−B7	B4, B7, B8	39.9, 55.7, 4.4	1.99	0.85	1.49	0.13
B5−B8	B4, B5, B8	6.6, 53.9, 39.4,	2.10	0.87	1.50	0.13
B4−B8	B4, B8	49.5, 50.3	2.19	0.89	1.51	0.16
B3−B7	Cu2, B3, B4, B7	1.7, 40.4, 8.7, 49.1	2.99	1.15	1.52	0.15
B5−B9	Cu1, B5, B9, B8	1.5, 49.0, 40.5, 8.9	3.03	1.16	1.52	0.15
B2−B9	Cu1, B2, B5, B6, B9	6.6, 48.3, 9.6, 3.6, 31.7	3.54	1.46	1.51	0.15
B3−B6	Cu2, B2, B3, B6, B7	6.3, 5.3, 30.9, 48.4, 8.9	3.62	1.49	1.51	0.15
B1−B3	B1, B3, B4	38.7, 42.0, 19.3	4.10	1.55	1.54	0.34
B9−B10	B8, B9, B10	19.2, 42.1, 38.7,	4.12	1.55	1.53	0.33
B1−B3	Cu1, B1, B2, B3	6.5, 33.2, 41.4, 19.0	4.90	1.83	1.53	1.15
B9−B10	Cu2, B6, B9, B10	6.8, 42.0, 19.3, 31.9	4.92	1.83	1.53	1.18
B1−B4	Cu1, B1, B4, B5	5.9, 35.5, 19.4, 39.1	5.23	1.94	1.53	1.19
B8−B10	Cu2, B7, B8, B10	5.4, 38.2, 19.9, 36.5	5.39	2.01	1.53	1.20
H7	Cu2, B7, H7	4.7, 12.5, 82.2	13.80	2.07	7.61	
H5	Cu1, B5, H5	6.2, 12.2, 81.2	14.01	2.07	7.46	
H6	Cu2, B6, H6	6.2, 12.2, 81.2	14.02	2.07	7.29	
H2	Cu1, B2, H2	5.9, 12.4, 81.4	14.12	2.07	7.46	
H1	Cu1, B1, H1	4.6, 14.5, 80.0	14.79	2.10	7.78	
H10	Cu2, B10, H10	4.5, 14.4, 80.3	14.97	2.10	7.83	

the weak influence of crystal packing effects on the bond topology. The $\rho(r)$ values at bcp's for B_a−B_e and B_e−B_e bonds (0.86 and 0.77 e Å^{-3}) as well as their ellipticities ($\varepsilon \approx 2.0$) are typical of deltahedral boranes.[3] The B−B bond of *cry* model match the relation of $\rho(r_{bcp})$ versus B−B bond lengths, which was found for other borane cages (Figure S1, Supporting Information).[9]

The bcp's corresponding to Cu−N and Cu−B bonds are characterized by positive values of $\nabla^2\rho(r)$ and negative values of local energy density ($H^e(r)$). Thus, the Cu−X bonds (X = N, H, B) are of the intermediate type. Intramolecular B−H···H−C, C−H···H−C and intermolecular interactions (listed in Table S1, Supporting Information) belong to closed-shell interactions ($H^e(r) > 0$ and $\nabla^2\rho(r) > 0$ at bcp). Ellipticity of Cu−N bonds does not exceed 0.12. That of B−B bonds varies from 1.2 to 2.1. In the case of interactions between a copper and a decaborate ellipticities are also high, especially in the case of Cu1−B1 bond in *cry* ($\varepsilon = 8.1$).

Table 3 lists the averaged descriptors of $\rho(r)$ at rcp for the rings bound with intramolecular bonds. Similar results of *gas* and *cry* models were averaged. Full list of "intramolecular" rcp is given in Table S2 (Supporting Information). The $\rho(r_{rcp})/\rho(r_{bcp})$ ratio for decaborate dianion varies from 0.8 to 0.9, a value much larger than that for aromatic or aliphatic rings. For both *gas* and *cry* models $\rho(r_{rcp})$, $\nabla^2\rho(r_{rcp})$, and λ_1 observed at rcp of four-membered B_{e1}−B_a−B_{e1}−B_{e2} rings are almost identical. At the same time the ring plane ellipticities [$\varepsilon_{rcp} = \lambda_2/\lambda_3 - 1$; $\lambda_2 > \lambda_3$] are alternated. Six of eight B−B−B−B rings are characterized by $\varepsilon_{rcp} = 0.4$−0.7. Ellipticities of B1−B2−B9−B5 and B10−B3−B6−B7 rings exceed 2. These are the rings involved in interactions with copper atoms. High ε_{bcp}(Cu−B) and ε_{rcp}(B−B−B−B) values reflect the fact of low curvature of the electron density in the regions of multicentered interactions. Corresponding λ values are $\sim 10^{-2}$, and in the case of Cu1−B1 bond in *cry* λ_1(bcp) $\sim 10^{-3}$. The ε_{bcp}(Cu1−B1) = 8.1 and ε_{rcp}(B1−B2−B9−B5) = 4.5 indicate that the system with the face coordination of decaborate by a copper atoms is more close to catastrophe point than the atomic system with the edge coordination.

Peculiarities of bonding situation in the region of copper and boron bonds can be visualized by means of Laplacian [$\nabla^2\rho(r)$] maps. The 2D Laplacian map in the Cu2−B6−B10 triangle

dx.doi.org/10.1021/jp405270u | J. Phys. Chem. A 2013, 117, 13138−13150

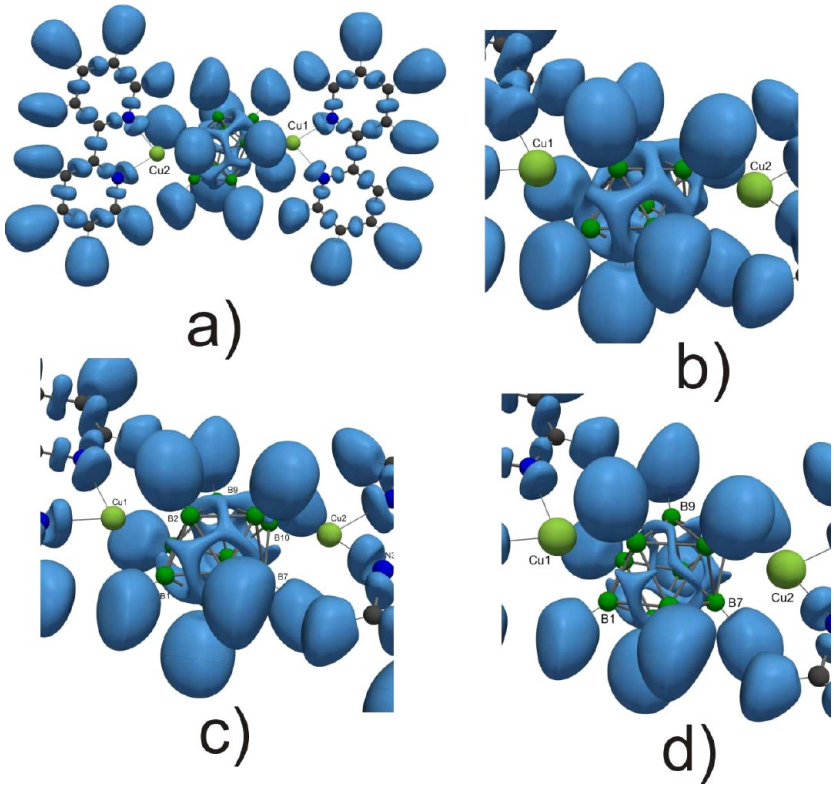

Figure 4. ELI-D isosurfaces for isolated **1**. General view of the molecule drawn at γ_D = 1.4 (a), and Cu−borane region drawn at γ_D = 1.3 (b), γ_D = 1.4 (c), and γ_D = 1.45 (d).

(Figure 3B) clearly shows the absence of charge concentrations orientated toward the metal atom. The electron density in the region of BB edges and BBB faces is very flat (Figure 3A). The absence of expected bond critical points was previously observed in a number of transition metal complexes with such π ligands as carbocyclic rings,[58,60] norbornadene[61] or 1-ethynyl-cyclohexan-1-ol.[62] Typically, the electron density function in the region of expected M−C bonds was found to be very flat, and the lack of some bcp's was related to a bond catastrophe having occurred. Hence, the results of topological analysis of ρ(r) of **1** expressed in usual form (molecular graph, atomic charges and the values of topological parameters in bcps, etc.) cannot be easily interpreted to obtain the clear chemical bonding pattern in d-metal polyborates and the bonding should be additionally characterized with other descriptors.

3.2.4. Integrated Bond Descriptors. The complementary analysis of the chemical bonding in **1** was carried out by means of the partitioning of ELI-D function. The ELI-D partitioning follows the similar rules used in AIM theory; however, it is also able to localize the domains that belong to bonded, core electrons, and lone electron pairs. The calculation of ELI-D function with subsequent integration was performed for the isolated molecule of **1**. The results are summarized in Table 4 and visualized at Figure 4. In principle, the electron populations and the corresponding volumes of ELI-D basins in $B_{10}H_{10}$ fragment are similar to that in the deltahedral boranes.[9,30] In the case of bipyridine molecules maxima of ELI-D function are located at the centers of C−C and C−N bonds. At the same time, the concentrations of ELI-D on coordination Cu−N bonds are shifted toward the N atoms. ELI-D distribution is quite different in the borane cage as compared to the bipyridines. The presented isosurfaces of ELI-D clearly show the delocalization of electron pair density in borane polyhedron. The maxima of ELI-D function are located in the centers of BBB triangles (in fact, they are close to the positions of CP(3,+1) in graphs of scalar fields of $\rho(r)$ and $V(r)$ functions). Besides, these maxima are not separated from each other; quite the opposite, they are connected by outstretched regions of ELI-D concentrations bisecting the B−B bonds in BBB triangles. Thus the regions of ELI-D concentrations form the network that covered the surface of the borane cage except for BBB triangles faced to the copper atoms. These triangles are characterized by noticeable depletion of ELI-D function. Possibly, the coordination of copper atoms to borane cage led to changes of the chemical bonding between boron atoms.

Topological analysis gave support to this assumption. The graph of ELI-D function resulted from the topological analysis is very complex (see Figure S2 in the Supporting Information), so the information from automatic procedure of basin determination was additionally verified by analysis of ELI-D and $\rho(r)$ basin intersections in the same way as ELF and $\rho(r)$ basin intersections.[64] The former method can be used as partitioning scheme to analyze the contributions of particular atoms to ELI-D basins that can be useful to understand character of multicenter bonds in polyhedral boranes. All basins corresponding to B−B bonding are characterized by disynaptic order as it was previously described in literature.[30,44] On the other hand, the characteristics of ELI-D basins vary in wide range, so the character of pair electron density distribution is quite different in particular BBB triangles. One can see that the value of ΔELI (the deviation of CP(3,−3) from the interatomic line) is increased along with the value of electronic population (ELI_{pop}). From this point of view all the bonds in the borane

dx.doi.org/10.1021/jp405270u | J. Phys. Chem. A 2013, 117, 13138−13150

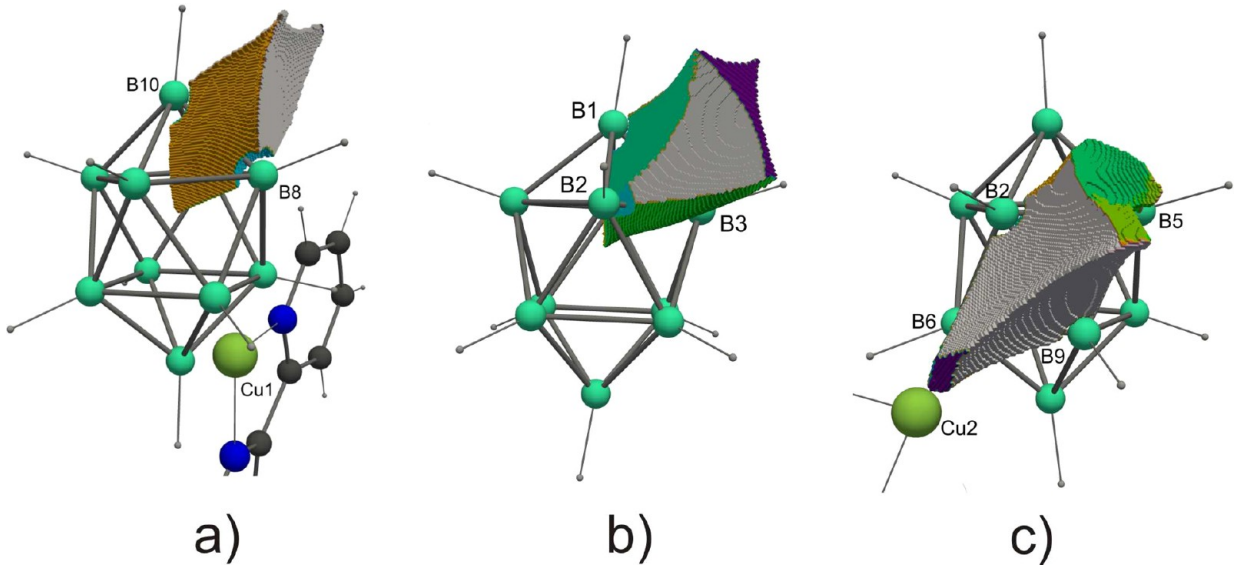

Figure 5. ELI-D basins responsible for chemical bonding in borane cage. The B8−B10 (a), B1−B3 (b), and B2−B9 (c) basins taken as examples of two-center, three-center, and multicenter bonding. Detailed characteristics can be found in Table 4.

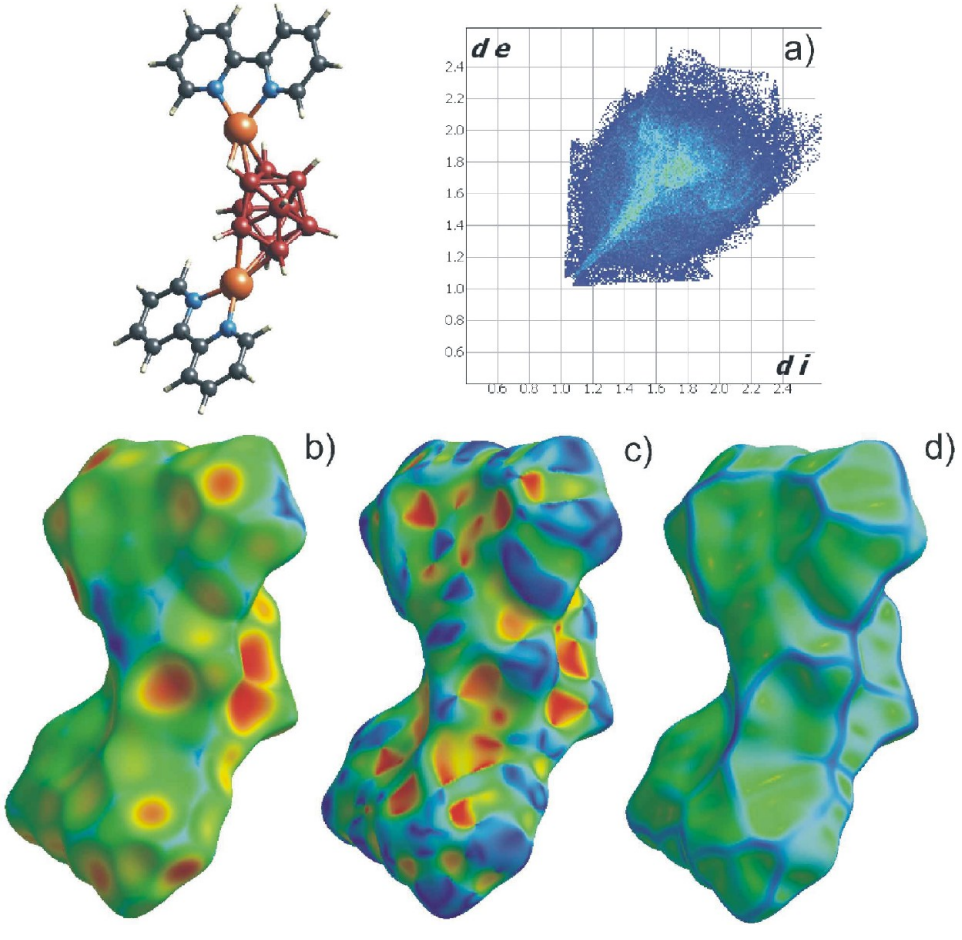

Figure 6. Hirshfeld surface for **1** and its 2D fingerprint plot (a). The surface is mapped with (b) d_e, (c) shape index, and (d) curvedness.

moiety are banana-type. Two first basins attributed to the electron pairs of apical B1 and B10 atoms and equatorial B4 and B8 ones are characterized by the lowest volume and ELI_{pop} (Table 4 and Figure 5a). Next four basins have almost the same values of ELI_{pop} and they belong to the equatorial boron atoms. In the case of B4−B7 and B5−B8 the small contribution of other atoms was revealed while the B2−B6 and B4−B8 correspond to "pure" two-center bonding. The B1−B3 and B9−B10 basins responsible for the bonding between apical and equatorial atoms are special case. In fact, the basins can be described as three-center bonds due to significant contribution of B4 and B8 atoms, respectively (Figure 5b).

dx.doi.org/10.1021/jp405270u | J. Phys. Chem. A 2013, 117, 13138−13150

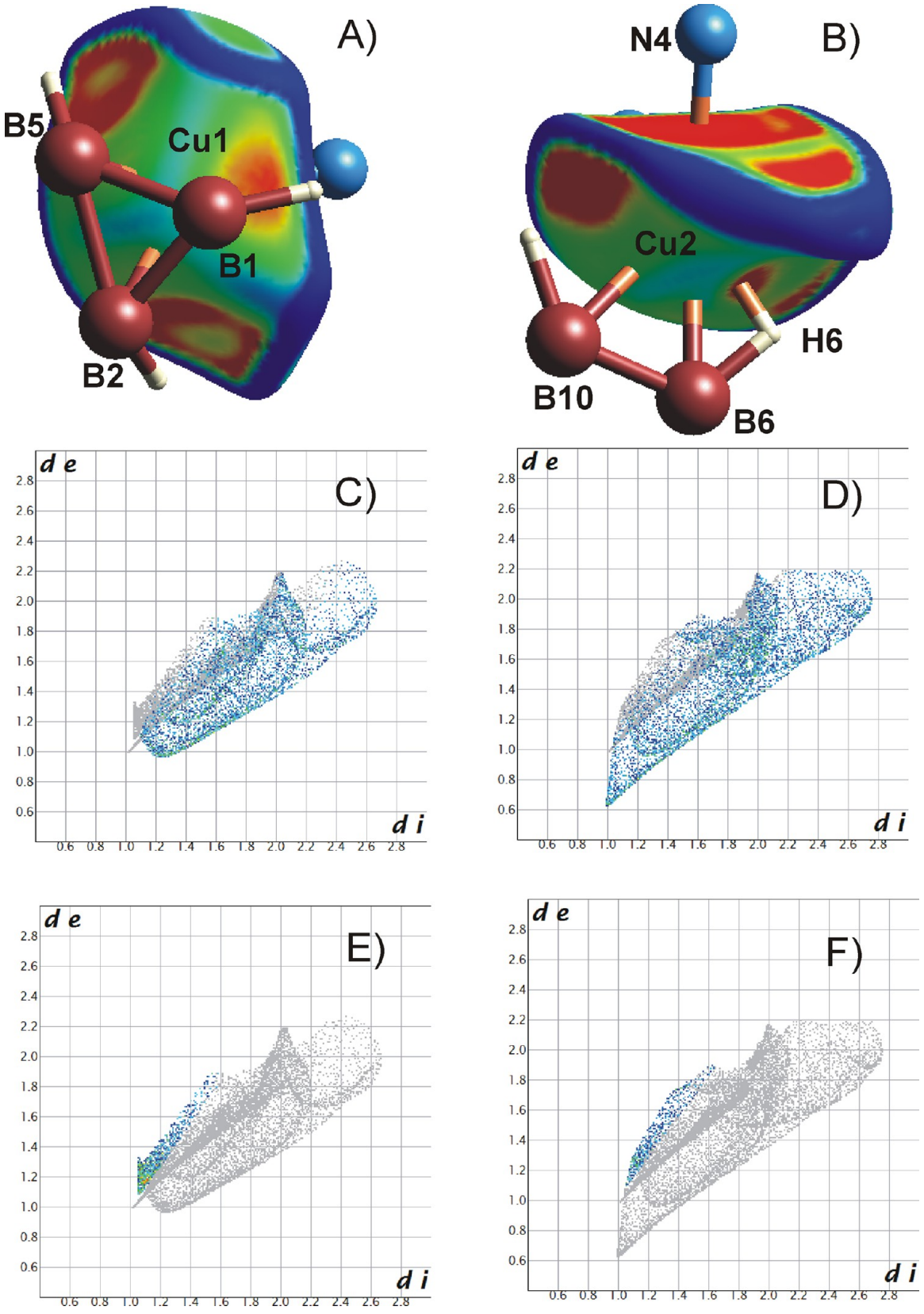

Figure 7. Curvedness plotted on the atomic Hirshfeld surfaces and mapped from −1.4 (flat; red) to −0.3 (sphere-like, blue) for the Cu1 (A) and Cu2 (B) atoms. The 2D fingerprint plots of interatomic interactions for the Cu1 (C, E) and Cu2 (D, F) atoms with Cu···H (C, E) or Cu···B interactions highlighted.

The rest of the B−B basins are characterized by large electronic populations that is an indicator of multicentered bonding. Remarkably, these basins are overlapped with $\rho(r)$ basins of copper atoms. The same situation is observed in the

dx.doi.org/10.1021/jp405270u | J. Phys. Chem. A 2013, 117, 13138−13150

case of formally monosynaptic basins of some hydrogen atoms. The extent of overlapping of B−B and H ELI-D basins with $\rho(r)$ basins of the copper atoms is rather small (1.5−6.8%). Besides, the topological analysis of ELI-D function revealed two additional Cu−B and one Cu−H disynaptic basins which can be, at first glance, responsible for the bonding between copper atoms and boron cage. On the contrary, these Cu−B and one Cu−H disynaptic basins fell inside the ρ(r) basins of copper atoms without overlapping with $\rho(r)$ basins of boron atoms (Figure S3, Supporting Information). There is no doubt that these basins belong to electrons of inner shells of copper atoms, and they cannot be responsible for Cu−borane bonding. Therefore, no 2c2e coordination bonds between copper atoms and the boron cage were revealed by analysis of ELI-D function. The multicenter bonding between the copper atoms, equatorial boron atoms, and some hydrogen atoms is observed instead. This bonding is rather weak, so the crystal packing can affect the position of copper atoms relatively to triangular BBB faces.

3.2.5. Hirshfeld Surface Analysis. Comparison of molecular graphs and bond distances for *gas* and *cry* models revealed redistribution of interatomic distances for both coordination centers (see section 3.2.2). In other words, geometry of coordination node was found to be labile. In the case of mono- and diprotonated decaborate dianion the barrier of edge-face migration of "additional" proton in the region of B_a atoms was found to be just 2−4 kcal/mol. Recently Juarez-Perez et al.[33] obtained that the *cisoid* conformation of C_2B_3 rings in the cobalt coordination node observed in the structure of $(NMe_4)[3,3'\text{-}Co(1,2\text{-}C_2B_9H_{11})_2]]$ is stabilized with H···H intermolecular interactions, although it is less stable than *transoid* disposition. Thus, it is not surprising that realization of numerous intermolecular bonds allows stabilization of face-edge coordination. Let us calculate the energies of intermolecular bonds using correlation formula proposed by Espinosa, et al.:[65]

$$E_{A\text{-}B} \approx -1/2V^e(r)$$

where $E_{A\text{-}B}$ is the energy of a weak interatomic contact or a coordination bond and $V^e(r)$ is potential energy density in the corresponding bcp. Taking all intermolecular contacts into account (Table S1, Supporting Information) one would obtain the sum energy of intermolecular contacts equal to 29 kcal/mol. This value is in good accord with packing energy of 26 kcal/mol calculated with intermolecular potentials using the 'UNI' force field.[66] Reorganization of electron density accompanied with crystal packing causes strengthening of Cu-*bipy* bonding (shortening of Cu−N bonds and increase in $\rho(r)$ at bcp's). What is more, additional packing energy facilities atomic movement in coordination node to relieve the stresses of catastrophe situation.

Peculiarities of supramolecular organization can be obtained using the Hirshfeld surface and its 2D fingerprint plot.[67−69] The 2D fingerprint plots provide a summary of the intermolecular interactions by mapping the fraction of points on the corresponding Hirshfeld surface as a function of the closest distances from the point to nuclei interior (d_i) and exterior (d_e) to the surface. The green region on the 2D plot (Figure 6a) with $d_i = d_e \approx 1.6 \div 1.9$ Å, as well as flat regions observed for curvedness above *bipy* molecules and red and blue triangles on the same region of the shape index surface (Figures 6c, 6d) indicate the presence of $\pi\cdots\pi$ interactions in crystalline **1**.[70] Indeed, six bcp's corresponding to C···C interactions with E_{bond} = 0.67−1.06 kcal/mol were found from PW-DFT data (Table S1, Figure S4, Supporting Information). Inspection of PW-DFT data revealed that the majority of intermolecular interactions in **1** are B−H···H−C followed by C−H···H−C ones (Table S1), those are observed in the region at (d_e; d_i) = (1.1−1.9; 1.1−1.9) Å of the 2D plot (Figure 6a).

To gain insight into copper···borate bonding, the atomic Hirshfeld surface (AHS) partitioning was also applied. Skovsen et al.[71] proposed that a low curvedness suggests close contacts and indicates covalent bonding situation. Although the AHS are calculated using neutral spherical atom charge densities, the volumes of copper atoms bounded by AHS (14.3 and 16.0 Å^3 for Cu1 and Cu2) are close to those of atomic domains surrounded by zero-flux surface (15.3 and 17.4 Å^3). In Figure 7 the curvedness of copper AHS is mapped over the range −1.4 to −0.3 (red is flat; blue is curved). Both copper atoms are not spherical. Flat red surfaces on these surfaces indicate strong interactions with nitrogen atoms of *bipy* molecules. Cu···borate bonding is characterized by more curved regions on AHSs, which is associated with presumably ionic interactions. The Cu1 atom has three flattened surfaces toward the boron claster (the Cu1−B1 surface is the most curved among them), and the Cu2 atom − toward two atoms of the claster. The AHS of copper atoms are significantly curved in the direction of Cu−B lines (green and blue regions). The flat surfaces attributed to Cu···borate bonding are directed to B−H bonds or H atoms. The 2D fingerprint plots of interatomic interactions in the region of copper atoms indicate that (d_e; d_i) distribution for Cu···B interactions is similar for two atoms. That for Cu···H interactions significantly differs due to the presence of a short Cu2−H6 distance (Figure 7).

3.2.6. Atomic Charges in gas and cry. The full list of AIM charges calculated for *cry* and *gas* models is listed in Table S3 (Supporting Information), and the averaged values for atoms with close charges are given in Table 5. The *cry* and *gas* calculated values are in a satisfactory agreement. We obtained positive charges for copper, boron, carbon, and H(C) atoms and negative charges for H(B) and nitrogen atoms. The values calculated for a *gas* model typically overpass those obtained within a *cry* model. As concerns the isolated molecule, both copper atoms and *bipy* molecules bear the same charges (0.67 and 0.09 e, respectively). In the case of a *cry* model, Bader charges of copper atoms slightly vary from each other (0.58 and 0.54 e for face- and egde-coordinated atoms). The decaborate is

Table 5. Selected AIM Charges for *cry* and *gas* Models[a]

atom	*cry*	*gas*	atom	*cry*	*gas*
Cu1	0.58	0.67	Cu2	0.54	0.67
B1	0.26	0.22	B6	0.32	0.42
H1	−0.55	−0.59	H6	−0.48	−0.58
B2	0.42	0.44	B7	0.48	0.60
H2	−0.55	−0.58	H7	−0.57	−0.59
B3	0.47	0.53	B8	0.54	0.40
H3	−0.56	−0.61	H8	−0.57	−0.59
B4	0.48	0.60	B9	0.46	0.59
H4	−0.57	−0.59	H9	−0.57	−0.61
B5	0.38	0.41	B10	0.25	0.20
H5	−0.52	−0.58	H10	−0.55	−0.59
C^a	0.46	0.53	$C^{\beta,\gamma}$	0.01	−0.02
N	−1.04	−1.21	H(C)	0.06	0.07

[a]AIM charge values for C, H(C), and N atoms were averaged.

negatively charged (−1.43/−1.52 e for *cry*/*gas*) with the apical BH groups being more negative (−0.30/−0.38 e in average) in comparison with equatorial ones (−0.10/−0.09 e). Hence, disposition of positively charged copper(I) atoms in the region of apical vertexes seem to be preferable in comparison with equatorial belt. Another interesting observation concerns variation of charges when passing from the isolated molecule to condensed matter. The charges of hydrogen atoms, B_a atoms, and carbon atoms not connected with nitrogen atoms, as well as that of *bipy* molecules in a whole remain almost constant. At the same time, variation of atomic charges of atoms involved in coordination bonding (all nitrogen atoms, carbon atoms connected with nitrogens, boron and hydrogen atoms involved in (CuHB) bonding) achieves 0.15 e. This fact also indicates electrostatic nature of chemical bonding in the region of copper bonds.

Singh and Patwari studied the C−H···H−B bonded systems to obtain that hydrogen atoms are oppositely charged.[72] The same observation can be done from our data. Hence, the majority of weak contacts appears between oppositely charged atoms (Table S3, Supporting Information). Nevertheless, a number of contacts should be referred to cation−cation (C···C, C−H···H−C, and B···H) or anion−anion (one B−H···N and one B−H···H−B, Table S1, Supporting Information) interactions.

The AIM charges were calculated by integration of $\rho(r)$ over the atomic basins surrounded by zero-flux surfaces. The same procedure can be carried out to obtain atomic volumes. The AIM volumes calculated for *cry* model are listed in Table S4, Supporting Information. The AIM volumes of *bipy* molecules coincide (191 Å^3), while the volume of more electropositive atom (Ω(Cu1) = 0.57 e) slightly overpass that of Cu2 (15.3 and 17.4 Å^3). It is interesting to note that estimation of atomic and molecular volumes by means of the Hirshfeld surfaces also gives good results. For example, the volumes of $B_{10}H_{10}^{2-}$ anion estimated within AIM and molecular Hirshfeld surfaces are equal to 188 and 177 Å^3, $V_{HS}(bipy)$ = 183 Å^3.

4. CONCLUSION

The chemical bonding between a copper(I), bipyridine molecules, and the decaborate dianion was investigated by means of QTAIM, ELI-D, and atomic Hirshfeld surface (AHS). It was discovered that the Cu−decaborate bonding is characterized with a zone of very flat $\rho(r)$ and very low $\nabla^2\rho(r)$. A clear distinction between 2c−2e and multicenter bonding was performed using intersection of $\rho(r)$ and ELI-D basins. The copper atoms are bonded to borane moiety via a number of weak Cu−B and Cu−H multicentered bonds. This is in agreement with AHS(Cu) curvedness and charge distribution, which indicate the predominantly electrostatic nature of Cu−borane bonding. As the result, disposition of copper(I) atoms above faces in the region of apical boron atoms seem to be preferable. Molecular and virial graphs represent a catastrophe situation in the region of the Cu−decaborate bonding, i.e., even tiny atomic displacement would be accompanied with reorganization of moleculare graph. Hence, description of this class of compounds in terms of individual bond paths is not satisfactory, and additional descriptors of chemical bonding should be applied.

■ ASSOCIATED CONTENT

Supporting Information

CIF file, details of synthetic procedure and FT-IR spectra, topological parameters of nonvalent interactions and ring critical points, atomic charges and volumes, atomic coordinates of optimized structure, and full list of authors for ref 53 are available free of charge via the Internet at http://pubs.acs.org.

■ AUTHOR INFORMATION

Corresponding Author

*E-mail: vologzhanina@mail.ru.

Notes

The authors declare no competing financial interest.

■ ACKNOWLEDGMENTS

The authors gratefully acknowledge support of the RFBR (Grants 12-03-331073, 12-03-31173, 13-03-00772, and 12-03-00878) and Council of the President of the Russian Federation (Grants MK-5181.2013.3 and MK-1728.2013.3).

■ REFERENCES

(1) Kuznetsov, N. T. Reactivity of Polyhedral Cluster Anions $(B_nH_n)^{2-}$ (n = 10, 12) as Spatial Aromatic Systems. *Russ. J. Inorg. Chem.* **2002**, *47*, 68.

(2) Brill, R.; Dietrich, H.; Dierks, H. Die Verteilung Der Bindungselektronen Im Dekaboran-molekül ($B_{10}H_{14}$). *Acta Crystallogr. B* **1971**, *27*, 2003−2018.

(3) Bader, R. F. W.; Legare, D. A. Properties of Atoms in Molecules: Structures and Reactivities of Boranes and Carboranes. *Can. J. Chem.* **1992**, *70*, 657−676.

(4) Jemmis, E. D.; Subramanian, G.; Srivastava, I. H.; Gadre, S. R. Closo-Boranes, -Carboranes, and -Silaboranes: A Topographical Study Using Electron Density and Molecular Electrostatic Potential. *J. Phys. Chem.* **1994**, *98*, 6445−6451.

(5) Lyssenko, K. A.; Antipin, M. Y.; Lebedev, V. N. Topological Analysis of the Electron Density Distribution in the Crystal of 8,9,10,12-Tetrafluoro-*o*-carborane on the Basis of the High-Resolution X-ray Diffraction Data at 120 K. *Inorg. Chem.* **1998**, *37*, 5834−5843.

(6) Panda, M.; Hofmann, K.; Prosenc, M. H.; Albert, B. Multi-centre, Hydrogen and Dihydrogen Bonds in Lithium Closo-hydroborate Obtained from Liquid Ammonia. *Dalton Trans.* **2008**, 3956−3958.

(7) Förster, D.; Scheins, S.; Luger, P.; Lentz, D.; Preetz, W. Electron Density and Bonding in Borates: An Experimental Study of Tetrabutylammonium Heptahydridohexaborate, $[(C_4H_9)_4N][B_6H_7]$. *Eur. J. Inorg. Chem.* **2007**, *2007*, 3169−3172.

(8) Kononova, E. G.; Leites, L. A.; Bukalov, S. S.; Pisareva, I. V.; Chizhevsky, I. T.; Kennedy, J. D.; Bould, J. Vibrational Spectrum and Electronic Structure of the $[B_{11}H_{11}]^{2-}$ Dianion. *Eur. J. Inorg. Chem.* **2007**, *2007*, 4911−4918.

(9) Mebs, S.; Kalinowski, R.; Grabowsky, S.; Förster, D.; Kickbusch, R.; Justus, E.; Morgenroth, W.; Paulmann, C.; Luger, P.; Gabel, D.; Lentz, D. Real-Space Indicators for Chemical Bonding. Experimental and Theoretical Electron Density Studies of Four Deltahedral Boranes. *Inorg. Chem.* **2011**, *50*, 90−103.

(10) Polyakova, I. N.; Malinina, E. A.; Kuznetsov, N. T. Crystal Structures of Cesium and Dimethylammonium Cupradecaborates, $Cs[CuB_{10}H_{10}]$ and $(CH_3)_2NH_2[CuB_{10}H_{10}]$. *Crystallogr. Rep.* **2003**, *48*, 84−91.

(11) Malinina, E.; Drozdova, V.; Polyakova, I.; Kuznetsov, N. Anionic Complexes of Cu(I) with the Closo-decaborate Anion. *Russ. J. Inorg. Chem.* **2008**, *53*, 197−201.

(12) Malinina, E. A.; Goeva, L. V.; Kuznetsov, N. T. Multicenter Interactions in lead(II) Coordination Compounds with $B_nH_n^{2-}$ n = 6, 10, 12) Cluster Anions and Their Derivatives. *Russ. J. Inorg. Chem.* **2009**, *54*, 417−424.

(13) Dobrott, R. D.; Lipscomb, W. N. Structure of $Cu_2B_{10}H_{10}$. *J. Chem. Phys.* **1962**, *37*, 1779−1784.
(14) Drozdova, V.; Malinina, E.; Kuznetsov, N. Isomerism of Metal Complexes with the Boron Cluster Anions $B_{10}H_{10}^{2-}$ and $B_{12}H_{12}^{2-}$. *Russ. J. Inorg. Chem.* **2009**, *54*, 1947−1951.
(15) McKee, M. L.; Buehl, M.; Charkin, O. P.; Schleyer, P. v. R. Theoretical Investigation of Four-center Two-electron Bonding Involving Boron Derivatives. *Inorg. Chem.* **1993**, *32*, 4549−4554.
(16) Mebel, A. M.; Charkin, O. P.; Buehl, M.; Schleyer, P. v. R. Structure and Nonrigidity of $B_{10}H_{11}^-$. An Ab initio/IGLO/NMR Study. *Inorg. Chem.* **1993**, *32*, 463−468.
(17) Shore, S. G.; Hamilton, E. J. M.; Bridges, A. N.; Bausch, J.; Krause-Bauer, J. A.; Dou, D.; Liu, J.; Liu, S.; Du, B.; Hall, H.; Meyers, E. A.; Vermillion, K. E. The Solid State Structure of $[B_{10}H_{11}]^-$ and Its Dynamic NMR Spectra in Solution. *Inorg. Chem.* **2003**, *42*, 1175−1186.
(18) Kochnev, V. K.; Avdeeva, V. V.; Malinina, E. A.; Kuznetsov, N. T. Theoretical Investigation of Dodecahydrodecaborane $B_{10}H_{12}$ - a Diprotonated Boron $B_{10}H_{10}^{2-}$ Claster. *Rus. J. Inorg. Chem.* **2013**, *58*, 793−799.
(19) Malinina, E. A.; Goeva, L. V.; Solntsev, K. A.; Kuznetsov, N. T. Cupra-decaborates of Alkali-metals and Alkylammonium. *Rus. J. Inorg. Chem.* **1993**, *38*, 38−41.
(20) Dziova, A. E.; Avdeeva, V. V.; Polyakova, I. N.; Malinina, E. A.; Rotov, A. V.; Efimov, N. N.; Minin, V. V.; Kuznetsov, N. T. Tetranuclear Hydroxo-bridged copper(II) Cluster of the Z Type: Preparation and Structural and Magnetic Characterization of $[(Cu_4bipy_4(OH)_4(B_{10}H_{10})_2(DMSO)_2]$. *Dokl. Chem.* **2012**, *442*, 1−3.
(21) Avdeeva, V. V.; Dziova, A. E.; Polyakova, I. N.; Goeva, L. V.; Malinina, E. A.; Kuznetsov, N. T. First Heterovalent Copper Complex with 2,2′-dipyridyl and Closo-decaborate Anion $B_{10}H_{10}^{2-}$. *Dokl. Chem.* **2011**, *437*, 79−81.
(22) Gill, J. T.; Lippard, S. J. Transition Metal Hydroborate Complexes. VIII. Structure of μ-decahydrodecaboratotetrakis-(triphenylphosphine)dicopper(I)-chloroform. Bonding Annalogies Between Boron Hydrides and Nido-metalloboranes. *Inorg. Chem.* **1975**, *14*, 751−761.
(23) Drozdova, V. V.; Malinina, E. A.; Polyakova, I. N.; Kuznetsov, N. T. Coordination Isomerism in Complexes of IB Group Metals with the Closo-decaborate Anion $B_{10}H_{10}^{2-}$ and Triphenylphosphine. *Dokl. Chem.* **2008**, *418*, 30−33.
(24) Dziova, A. E.; Avdeeva, V. V.; Polyakova, I. N.; Goeva, L. V.; Malinina, E. A.; Kuznetsov, N. T. Boron Cluster Anions $B_{10}H_{10}^{2-}$ and $B_{10}H_{11}^-$ in Complexation Reactions of Copper(I). Positional Isomers of the Complex $[Cu_2(9Nphen)_4B_{10}H_{10}]$. *Russ. Chem. Bull.* **2011**, *60*, 1608−1611.
(25) Vologzhanina, A. V.; Avdeeva, V. V.; Malinina, E. A.; Kuznetsov, N. T. Synthesis and Crystal Structure of Poly-(tetraphenylphosphonium (μ2-closo-decaborato)copper(I)). *Z. Kristallogr.* **2013**, DOI: 10.1524/zkri.2013.1647.
(26) Bader, R. F. W. *Atoms in Molecules. A Quantum Theory*; Clarendon Press: Oxford, U.K., 1990.
(27) Becke, A. D.; Edgecombe, K. E. A Simple Measure of Electron Localization in Atomic and Molecular Systems. *J. Chem. Phys.* **1990**, *92*, 5397.
(28) Kohout, M. A Measure of Electron Localizability. *Int. J. Quantum Chem.* **2004**, *97*, 651−658.
(29) Lyssenko, K. A.; Golovanov, D. G.; Meshcheryakov, V. I.; Kudinov, A. R.; Antipin, M. Yu. Nature of Weak Inter- and Intramolecular Interactions in Crystals. 5. Interactions Na···H—B in a Crystal of Sodium Salt of Charge-compensated Nido-carborane $[9\text{-}SMe2\text{-}7,8\text{-}C_2B_9H_{10}]^-$. *Russ. Chem. Bull.* **2005**, *54*, 933−941.
(30) Mebs, S.; Kalinowski, R.; Grabowsky, S.; Förster, D.; Kickbusch, R.; Justus, E.; Morgenroth, W.; Paulmann, C.; Luger, P.; Gabel, D.; Lentz, D. Charge Transfer via the Dative N−B Bond and Dihydrogen Contacts. Experimental and Theoretical Electron Density Studies of Four Deltahedral Boranes. *J. Phys. Chem. A* **2011**, *115*, 1385−1395.
(31) Antipin, M.; Boese, R.; Bläser, D.; Maulitz, A. Molecular Crystal Structure and Electron Density Distribution in the Crystal of Pentaethyl-1,5-dicarba-closo-pentaborane $[C_2B_3(Et)_5]$ at 120 K. *J. Am. Chem. Soc.* **1997**, *119*, 326−333.
(32) Mollendal, H.; Samdal, S.; Holub, J.; Hnyk, D. The Structure of 1-thia-closo-decaborane(9), 1-SB_9H_9, as Determined by Microwave Spectroscopy and Quantum Chemical Calculations. *Inorg. Chem.* **2002**, *41*, 4574−4578.
(33) Juarez-Pérez, E. J.; Núñez, R.; Viñas, C.; Sillanpää, R.; Teixidor, F. The Role of C−H···H−B Interactions in Establishing Rotamer Configurations in Metallabis(dicarbollide) Systems. *Eur. J. Inorg. Chem.* **2010**, *2010*, 2385−2392.
(34) Alekseev, L. S.; Safronov, A. V.; Dolgushin, F. M.; Korlyukov, A. A.; Godovikov, I. A.; Chizhevsky, I. T. An Unexpected Cluster Opening Upon the Formation of Electronically Unsaturated H3-(cyclooctenyl)metallacarboranes of rhodium(III) and iridium(III) with Sterically Reduced $[(PhCH_2)_2C_2B_9H_9]^{2-}$ Ligand. *J. Organomet. Chem.* **2009**, *694*, 1727−1735.
(35) Bould, J.; Harrington, R. W.; Clegg, W.; Kennedy, J. D. Nine-vertex Metallaborane Chemistry. Preparation and Characterisation of $[1,1,1\text{-}(PMe_3)_2H\text{-}isocloso\text{-}IrB_8H_7\text{-}8\text{-}X]$, Where X = H or Cl. *J. Organomet. Chem.* **2012**, *721*−*722*, 155−163.
(36) Boucher, B.; Ghosh, S.; Halet, J.-F.; Kahlal, S.; Saillard, J.-Y. Bonding and Electronic Structure of $Cp^*_2Ru_2(B_8H_{14})$, a Metal-laborane Analogue of Dinuclear Pentalene Complexes. *J. Organomet. Chem.* **2012**, *721*−*722*, 167−172.
(37) Scott, G.; Ellis, D.; Rosair, G. M.; Welch, A. J. Icosahedral and Supraicosahedral Naphthalene Ruthenacarboranes. *J. Organomet. Chem.* **2012**, *721*−*722*, 78−84.
(38) Scott, G.; McAnaw, A.; McKay, D.; Boyd, A. S. F.; Ellis, D.; Rosair, G. M.; Macgregor, S. A.; Welch, A. J.; Laschi, F.; Rossi, F.; Zanello, P. Supraicosahedral Indenyl Cobaltacarboranes. *Dalton Trans.* **2010**, *39*, 5286−5300.
(39) Pandey, K. K. What Is the Best Bonding Model of the (σ-H-BR) Species Bound to a Transition Metal? Bonding Analysis in Complexes $[(H)_2Cl(PMe_3)_2M(\sigma\text{-}H\text{-}BR)]$ (M = Fe, Ru, Os). *Dalton Trans* **2012**, *41*, 3278−3286.
(40) Burkhardt, A.; Wedig, U.; von Schnering, H. G.; Savin, A. Die Elektronen-Lokalisierungs-Funktion in closo-Bor-Clustern. *Z. Anorg. Allg. Chem.* **1993**, *619*, 437−441.
(41) Binder, H.; Kellner, R.; Vaas, K.; Hein, M.; Baumann, F.; Wanner, M.; Kaim, W.; Wedig, U.; Hönle, W.; von Schnering, H. G.; Groeger, O.; Engelhardt, G. $HB_9X_9^-$ and $H_2B_9X_9$ (X = Cl, Br, I): Neutral *closo*-Nonaboranes in the Novel Series B_nH_{n+1}, and B_nH_{n+2} − Syntheses, Ab Initio Calculations, and Electronic Structures. *Z. Anorg. Allg. Chem.* **1999**, *625*, 1638−1646.
(42) Yamaguchi, M.; Ohishi, Y.; Hosoi, S.; Soga, K.; Kimura, K. Metallic-covalent Bonding Conversion in Boron Icosahedral Cluster Solids Studied Using Electron Localizability Indicator. *J Phys Conf Ser* **2009**, *176*, 012027.
(43) Börrnert, C.; Grin, Y.; Wagner, F. R. Position-Space Bonding Indicators for Hexaborides of Alkali, Alkaline-Earth, and Rare-Earth Metals in Comparison to the Molecular Crystal $K_2[B_6H_6]$. *Z. Anorg. Allg. Chem.* **2013**, *639*, 2013−2024.
(44) Mebs, S.; Henn, J.; Luger, P.; Lentz, D. Theoretical AIM and ELI-D Study of Ammonium Hexahydrohexaborate. *Z. Anorg. Allg. Chem.* **2013**, *639*, 2057−2064.
(45) Miller, H. C.; Miller, N. E.; Muetterties, E. L. Synthesis of Polyhedral Boranes. *J. Am. Chem. Soc.* **1963**, *85*, 3885−3886.
(46) Ochertyanova, L. I.; Mustyatsa, V. N.; Zhizhin, K. Y.; Belousova, O. N.; Kuznetsov, N. T. Synthesis and Composition of Compounds Containing the $B_{10}H_{11}$ Anion. *Inorg. Mater.* **2004**, *40*, 144−146.
(47) Sheldrick, G. A short history of SHELX. *Acta Crystallogr.* **2008**, *A64*, 112−122.
(48) Kresse, G.; Hafner, J. Ab Initio Molecular Dynamics for Liquid Metals. *Phys. Rev. B* **1993**, *47*, 558.
(49) Kresse, G.; Furthmüller, J. Efficient Iterative Schemes for Ab Initio Total-energy Calculations Using a Plane-wave Basis Set. *Phys. Rev. B* **1996**, *54*, 11169.

(50) Kresse, G.; Furthmüller, J. Efficiency of Ab-initio Total Energy Calculations for Metals and Semiconductors Using a Plane-wave Basis Set. *Comput. Mater. Sci.* **1996**, *6*, 15−50.
(51) Perdew, J. P.; Burke, K.; Ernzerhof, M. Generalized Gradient Approximation Made Simple. *Phys. Rev. Lett.* **1996**, *77*, 3865.
(52) Gonze, X.; Beuken, J.-M.; Caracas, R.; Detraux, F.; Fuchs, M.; Rignanese, G.-M.; Sindic, L.; Verstraete, M.; Zerah, G.; Jollet, F.; Torrent, M.; Roy, A.; Mikami, M.; Ghosez, P.; Raty, J.-Y.; Allan, D. C. First-principles Computation of Material Properties: The ABINIT Software Project. *Comput. Mater. Sci.* **2002**, *25*, 478−492.
(53) Frisch, M. J., et al. *Gaussian 03*, revision C.01; Gaussian Inc: Wallingford CT, 2004.
(54) Keith, T. A. AIMAll (Version 09.04.23) 2009.
(55) Kohout, M. *Programs DGrid and Basin*. http://www.cpfs.mpg.de/∼kohout/dgrid.html, 2005.
(56) Henderson, A.; Ahrens, J.; Law, C. *The ParaView Guide*; Kitware, Inc.: Clifton Park, NY, 2004.
(57) Keith, T. A.; Bader, R. F. W.; Aray, Y. Structural Homeomorphism Between the Electron Density and the Virial Field. *Int. J. Quantum Chem.* **1996**, *57*, 183−198.
(58) Farrugia, L. J.; Evans, C.; Lentz, D.; Roemer, M. The QTAIM Approach to Chemical Bonding Between Transition Metals and Carbocyclic Rings: A Combined Experimental and Theoretical Study of $(\eta^5\text{-}C_5H_5)Mn(CO)_3$, $(\eta^6\text{-}C_6H_6)Cr(CO)_3$, and (E)-$(\eta^5\text{-}C_5H_4)CF{=}CF(\eta^5\text{-}C_5H_4)(\eta^5\text{-}C_5H_5)_2Fe_2$. *J. Am. Chem. Soc.* **2009**, *131*, 1251−1268.
(59) Mebs, S.; Chilleck, M. A.; Grabowsky, S.; Braun, T. Hapticity Uncovered: Real-Space Bonding Indicators for Zincocene Chemistry. *Chem.−Eur. J.* **2012**, *18*, 11647−11661.
(60) Firme, C. L.; Pontes, D. de L.; Antunes, O. A. C. Topological Study of Bis(cyclopentadienyl) Titanium and Bent Titanocenes. *Chem. Phys. Lett.* **2010**, *499*, 193−198.
(61) Sparkes, H. A.; Brayshaw, S. K.; Weller, A. S.; Howard, J. A. K. $[Rh(C_7H_8)(PPh_3)Cl]$: an experimental charge-density study. *Acta Crystallogr.* **2008**, *B64*, 550−557.
(62) Overgaard, J.; Clausen, H. F.; Platts, J. A.; Iversen, B. B. Experimental and Theoretical Charge Density Study of Chemical Bonding in a Co Dimer Complex. *J. Am. Chem. Soc.* **2008**, *130*, 3834−3843.
(63) Biegler-Konig, F.; Schonbohm, J. Update of the AIM2000-program for Atoms in Molecules. *J. Comput. Chem.* **2002**, *23*, 1489−1494.
(64) Raub, S.; Jansen, G. A Quantitative Measure of Bond Polarity from the Electron Localization Function and the Theory of Atoms in Molecules. *Theor. Chem. Acc.* **2001**, *106*, 223−232.
(65) Espinosa, E.; Molins, E.; Lecomte, C. Hydrogen Bond Strengths Revealed by Topological Analyses of Experimentally Observed Electron Densities. *Chem. Phys. Lett.* **1998**, *285*, 170−173.
(66) Gavezzotti, A. Calculation of lattice energies of organic crystals: the PIXEL integration method in comparison with more traditional methods. *Z. Kristallogr.* **2005**, *220*, 499−510.
(67) Spackman, M. A.; Jayatilaka, D. Hirshfeld Surface Analysis. *CrystEngComm* **2009**, *11*, 19−32.
(68) Spackman, M. A.; McKinnon, J. J. Fingerprinting Intermolecular Interactions in Molecular crystals. *CrystEngComm* **2002**, *4*, 378.
(69) *CrystalExplorer* (Version 3.0), Wolff, S.K.; Grimwood, D.J.; McKinnon, J.J.; Turner, M.J.; Jayatilaka, D.; Spackman, M.A., University of Western Australia, 2012.
(70) McKinnon, J. J.; Spackman, M. A.; Mitchell, A. S. Novel tools for visualizing and exploring intermolecular interactions in molecular crystals. *Acta Crystallogr.* **2004**, *B60*, 627−668.
(71) Skovsen, I.; Christensen, M.; Clausen, H. F.; Overgaard, J.; Stiewe, C.; Desgupta, T.; Mueller, E.; Spackman, M. A.; Iversen, B. B. Synthesis, Crystal Structure, Atomic Hirshfeld Surfaces, and Physical Properties of Hexagonal $CeMnNi_4$. *Inorg. Chem.* **2010**, *49*, 9343−9349.
(72) Singh, P. C.; Naresh Patwari, G. The C−H···H−B Dihydrogen Bonded Borane-trimethylamine Dimer: A Computational Study. *Chem. Phys. Lett.* **2006**, *419*, 265−268.